


Structural and catalytic roles of the human 18S rRNA methyltransferases DIMT1 in ribosome assembly and translation

Received for publication, May 5, 2020, and in revised form, June 26, 2020. Published, Papers in Press, July 2, 2020, DOI 10.1074/jbc.RA120.014236

Hui Shen¹, Julian Stoute^{1,2}, and Kathy Fange Liu^{1,2,*} 

From the ¹Department of Biochemistry and Biophysics, Perelman School of Medicine, University of Pennsylvania, Philadelphia, Pennsylvania, USA, and ²Graduate Group in Biochemistry and Molecular Biophysics, Perelman School of Medicine, University of Pennsylvania, Philadelphia, Pennsylvania, USA

Edited by Ronald C. Wek

rRNA-modifying enzymes participate in ribosome assembly. However, whether the catalytic activities of these enzymes are important for the ribosome assembly and other cellular processes is not fully understood. Here, we report the crystal structure of WT human dimethyladenosine transferase 1 (DIMT1), an 18S rRNA *N*^{6,6}-dimethyladenosine (*m*₂^{6,6}A) methyltransferase, and results obtained with a catalytically inactive DIMT1 variant. We found that *DIMT1*^{+/-} heterozygous HEK 293T cells have a significantly decreased 40S fraction and reduced protein synthesis but no major changes in *m*₂^{6,6}A levels in 18S rRNA. Expression of a catalytically inactive variant, DIMT1-E85A, in WT and *DIMT1*^{+/-} cells significantly decreased *m*₂^{6,6}A levels in 18S rRNA, indicating a dominant-negative effect of this variant on *m*₂^{6,6}A levels. However, expression of the DIMT1-E85A variant restored the defects in 40S levels. Of note, unlike WT DIMT1, DIMT1-E85A could not revert the defects in protein translation. We found that the differences between this variant and the WT enzyme extended to translation fidelity and gene expression patterns in DNA damage response pathways. These results suggest that the catalytic activity of DIMT1 is involved in protein translation and that the overall protein scaffold of DIMT1, regardless of the catalytic activity on *m*₂^{6,6}A in 18S rRNA, is essential for 40S assembly.

Ribosomes are molecular machines that are essential for protein synthesis. In eukaryotes, ribosome assembly requires four ribosomal RNAs (18S, 5.8S, 25S, and 5S) (1–4) as well as ~200 indispensable assembly factors. Many of these factors play a role in the cleavage of rRNA precursor transcripts, folding of rRNA, facilitating the binding of ribosomal proteins, and catalyzing rRNA modifications (1–5).

Several rRNA-modifying enzymes participate in ribosome biogenesis (3, 6, 7). Among these rRNA-modifying enzymes, dimethyladenosine transferase 1 (DIMT1), an SAM-dependent methyltransferase, installs *N*^{6,6}-dimethyladenosine (*m*₂^{6,6}A) at the two adjacent adenosine sites A1850 and A1851 in human 18S rRNA (Fig. S1, A and B) (8–12). DIMT1-catalyzed *m*₂^{6,6}A sites in 18S rRNA are conserved in all three kingdoms of life (Fig. 1A) (8, 13). As shown in a cryo-EM structure of the human ribosome (PDB entry 6EK0) (4), the adjacent *m*₂^{6,6}A sites reside between

the 40S and 60S subunits and directly interact with tRNA (P- and E-sites) and mRNA on the ribosome (Fig. S1B). The structural studies of the ribosomal complex suggest that DIMT1 functions as a checkpoint protein in translation by interacting with small subunits of the ribosome and precluding eIF1A from engaging in pre-mature translation (1, 14, 15).

The biological significance of the DIMT1-mediated *m*₂^{6,6}A in 18S rRNA was previously explored by the knockout studies of DIMT1 in multiple species, including bacteria, budding yeast, and *Arabidopsis thaliana*. The DIMT1 knockout leads to increased sensitivity of these organisms to stress conditions (16–18). Interestingly, previous studies suggested that the expression, but not the catalytic activity, of DIMT1 is important for rRNA processing and ribosome biogenesis (19). Bacteria with catalytically dead KsgA are more sensitive to antibiotics (20); however, in yeast, the catalytically inactive DIMT1 variants do not lead to obvious growth defects compared with the wild type (WT) strain (17). Sporadic studies of human DIMT1 suggested that DIMT1 is important for the regulation of cell proliferation in cancer (21–24). Elevated levels of DIMT1 correlate with the progression of multiple myeloma and colon cancer (21–24); however, the molecular mechanism is not understood. The only study to investigate the mechanism by which human DIMT1 influences 18S rRNA processing showed that the catalytic activity of DIMT1 is not required for this process, leaving the function of the evolutionarily conserved rRNA modification *m*₂^{6,6}A uncharacterized (19).

Whereas the finding of a noncatalytic structural role for DIMT1 is highly credible, no evidence suggests that the catalytic role of DIMT1 is required for ribosome biogenesis or protein translation (10, 25–29). In addition, whereas the mechanisms regulating partial modification and the functions of specialized ribosomes are largely unknown, changes in the rRNA modification pattern have been observed in response to environmental changes, during development, and in disease. Most of the studies of rRNA modifications were carried in the bacterial and yeast systems. In human cells, the best-characterized rRNA modifications are 2'-*O*-methylation and pseudouridylation (30–32). Dysregulation of these two rRNA modifications can affect ribosome ligand binding and translation fidelity (30, 32). However, the biological functions of most of the rRNA modifications, especially in mammalian systems, remains elusive.

This article contains supporting information.

* For correspondence: Kathy Fange Liu, liufg@penmedicine.upenn.edu.

This is an Open Access article under the CC BY license.

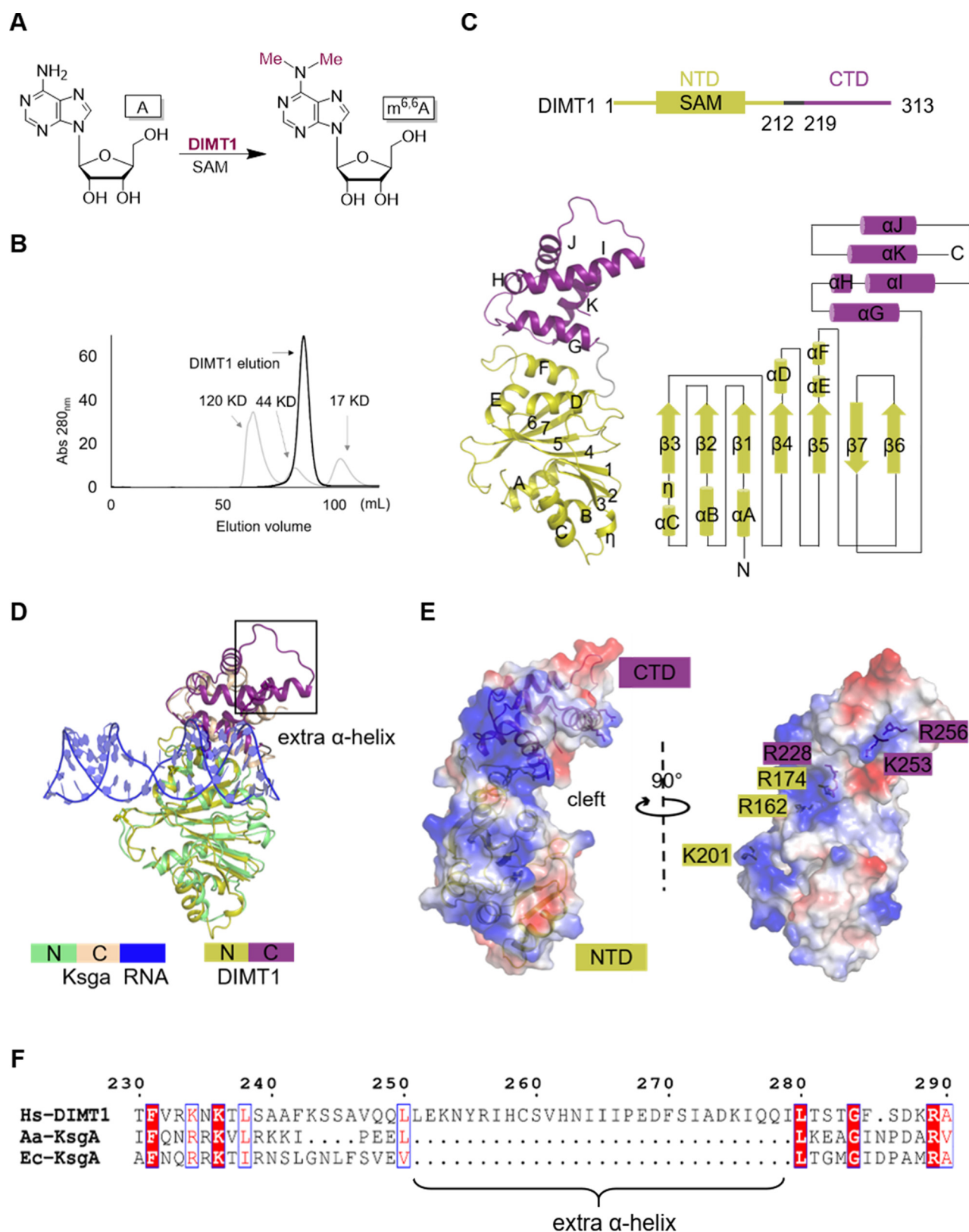


Figure 1. Crystal structure of human DIMT1. A, DIMT1-catalyzed methylation reaction. B, gel filtration elution profile of DIMT1. Elution of three standard proteins is shown in gray lines, whereas DIMT1 is shown in a black line. C, DIMT1 contains two domains. Shown is a ribbon representation of human DIMT1, with the β -strands and α -helices numbered numerically and alphabetically, respectively, and a schematic representation of the structure of human DIMT1. D, overlapped structures of KsgA in complex with RNA and human DIMT1. Each domain of KsgA and human DIMT1, as well as the RNA, are individually color coded. E, electrostatic surface of human DIMT1. The six positive-charged residues that potentially interact with the RNA substrates are annotated. F, sequence alignment of human DIMT1 and KsgA showing an additional α -helix in human DIMT1.

Catalytic-dependent and -independent roles of human DIMT1

Here, we characterize the structure and molecular functions of human DIMT1. The results reveal that residue Glu85 is important for DIMT1-mediated $m_2^{6,6}$ A installation. We studied and compared the effects of *DIMT1*^{+/-} heterozygous cells and the catalytically inactive DIMT1 E85A variant on ribosome assembly and protein translation. Collectively, our results suggest the importance of the roles of both the noncatalytic structural scaffold and the catalytic activity of DIMT1 in these processes.

Results

Structural characterization of WT and variant human DIMT1

To gain a molecular-level understanding of DIMT1, we determined the three-dimensional structure of DIMT1 through X-ray crystallography. We used a previously deposited but not published structure of human DIMT1 (PDB entry 1ZQ9) as the template in molecular replacement in our study. The crystal structure was finally refined to 2.38-Å resolution with 99.4% completeness. The structure of DIMT1 belongs to space group *P*₂₁₂₁₂₁. Data collection and refinement statistics are listed in Table S1. This structure reveals two DIMT1 copies in the asymmetric unit, whereas DIMT1 exists as a monomer in solution (Fig. 1B and Fig. S1C). The N-terminal domain (NTD) exhibits the SAM-dependent MTase fold, which is reminiscent of the Rossmann fold, with a central seven-stranded β sheet flanked by three α helices on each side (Fig. 1C). The C-terminal domain (CTD), located on one side of the β sheet, is composed of five α helices, which are linked to NTD by a loop (212–219) (Fig. 1C). There is a cleft between NTD and CTD, lined with α helix D, E, and F in the NTD and G and I in the CTD. The cleft is positively charged, providing a potential platform to bind RNA (Fig. 1, D and E). The structure of KsgA (PDB entry 3FTE), a prokaryotic homolog of DIMT1, in complex with a dsRNA has already been determined (11). Although DIMT1 and KsgA have limited sequence identity (26.05%, calculated using Clustal2.1 [33]), DIMT1 and KsgA have similar overall structures with a root mean square deviation (r.m.s.d.) of 1.518 Å for 147 residues. Although the structural similarities of the NTDs of DIMT1 and of KsgA are extremely close, there is an extra α helix (helix I) in the CTD of DIMT1 (Fig. 1D). This extra α helix provides multiple interactions with the RNA substrate. Moreover, sequence alignment showed that this α helix is conserved in several eukaryotic species although absent from prokaryotes (Fig. 1F). This implies that these dimethyladenosine methyltransferases have different substrate affinity or selectivity between eukaryotes and prokaryotes. The structure we determined also reveals that several positively charged side chains on both sides of the cleft in human DIMT1 are potentially important for binding of the substrate RNA. We observe the residues Arg162, Arg174, and Lys201 in the NTD and Arg228, Lys253, and Arg256 in the CTD of DIMT1. Of note, both Lys253 and Arg256 are in the α helix I of DIMT1 (Fig. 1E).

DIMT1 deficiency leads to decreased protein translation

We next studied whether the deficiency in DIMT1 leads to defects in 40S assembly. Thus, we attempted to generate *DIMT1* KO by employing CRISPR/Cas9. We screened for *DIMT1*^{-/-}

homozygous knockout single colonies by using several pairs of designed PCR primers covering the CRISPR cut sites (Fig. 2A). However, all the single colonies we obtained were heterozygous with cut and uncut DIMT1 alleles (*DIMT1*^{+/-}) (Fig. S2B). These results suggest that DIMT1 is essential for HEK293T cell viability. Thus, we selected two *DIMT1*^{+/-} single colonies from the CRISPR/Cas9 screening and confirmed their genotype using Sanger sequencing experiments (Fig. S2, C and D). Western blotting results revealed that the protein levels of DIMT1 significantly decrease in the *DIMT1*^{+/-} single colonies compared with those in the WT cells (Fig. 2A).

Next, we quantified the $m_2^{6,6}$ A levels in 18S rRNA extracted from WT and *DIMT1*^{+/-} heterozygous cell lines using liquid chromatography triple-quadrupole MS (LC-MS/MS). Unsurprisingly, the results showed that heterozygous *DIMT1*^{+/-} does not lead to obvious changes in the $m_2^{6,6}$ A levels in 18S rRNA (Fig. 2B and Fig. S3), which was seen in other RNA-modifying enzyme heterozygous cells. We also performed transient knockdown of DIMT1 and a knockdown control for 48 h, reaching a knockdown efficiency of ~95%. However, the LC-MS/MS results showed that DIMT1 transient knockdown does not change $m_2^{6,6}$ A levels in 18S rRNA (Fig. S4, A and B). This is likely because of the long lifetime of 18S rRNA (34). Strikingly, heterozygous *DIMT1*^{+/-} displays a significantly decreased 40S level in polysome profiling when comparing the ratio of 40S peaks to 60S peaks (Fig. 2C and Fig. S4C), which is likely through the decreased protein level of DIMT1. We observed decreased cell proliferation in *DIMT1*^{+/-} heterozygous compared with WT cells (Fig. 2D). These results are consistent with the fact that DIMT1 is important for 18S rRNA processing and the biogenesis of the small subunit in the ribosome (6, 7, 19).

To understand whether DIMT1 deficiency leads to defects in protein translation, we performed pulse-chase labeling experiments using the unnatural amino acid homopropargylglycine (HPG) for metabolic labeling of newly synthesized proteins. WT and *DIMT1*^{+/-} cells were incubated with HPG, which was further fluorescently labeled. The results showed that *DIMT1*^{+/-} cells have a significant decrease in global protein translation compared with the WT cells (Fig. 2E). We also employed an *in vitro* translation system to quantify the protein synthesis in WT and *DIMT1*^{+/-} cells. In detail, cells were first lysed under hypotonic conditions to keep the integrity and activity of the translation machinery of WT and *DIMT1*^{+/-} cells. A firefly luciferase mRNA and necessary cofactors (*i.e.* ATP and GTP) were added to allow *in vitro* translation to occur. This system can mimic the cellular translation (35). As shown in Fig. 2F, *DIMT1*^{+/-} led to an ~55% decrease in protein translation. Furthermore, we performed *in vivo* protein synthesis assays by incubating live cells with puromycin to label nascent peptides and traced peptide production via Western blotting, and GAPDH was used as a loading control. As shown in Fig. 2G, the results are consistent with the results from the HPG assays and the *in vitro* translation experiments, indicating that *DIMT1*^{+/-} exhibits significantly decreased protein synthesis. The same experiment was carried out in DIMT1 knockdown and knockdown control cells. The results showed that DIMT1 knockdown leads to an ~45% reduction of puromycin signal compared to that of the knockdown control cells (Fig. S4D). These results

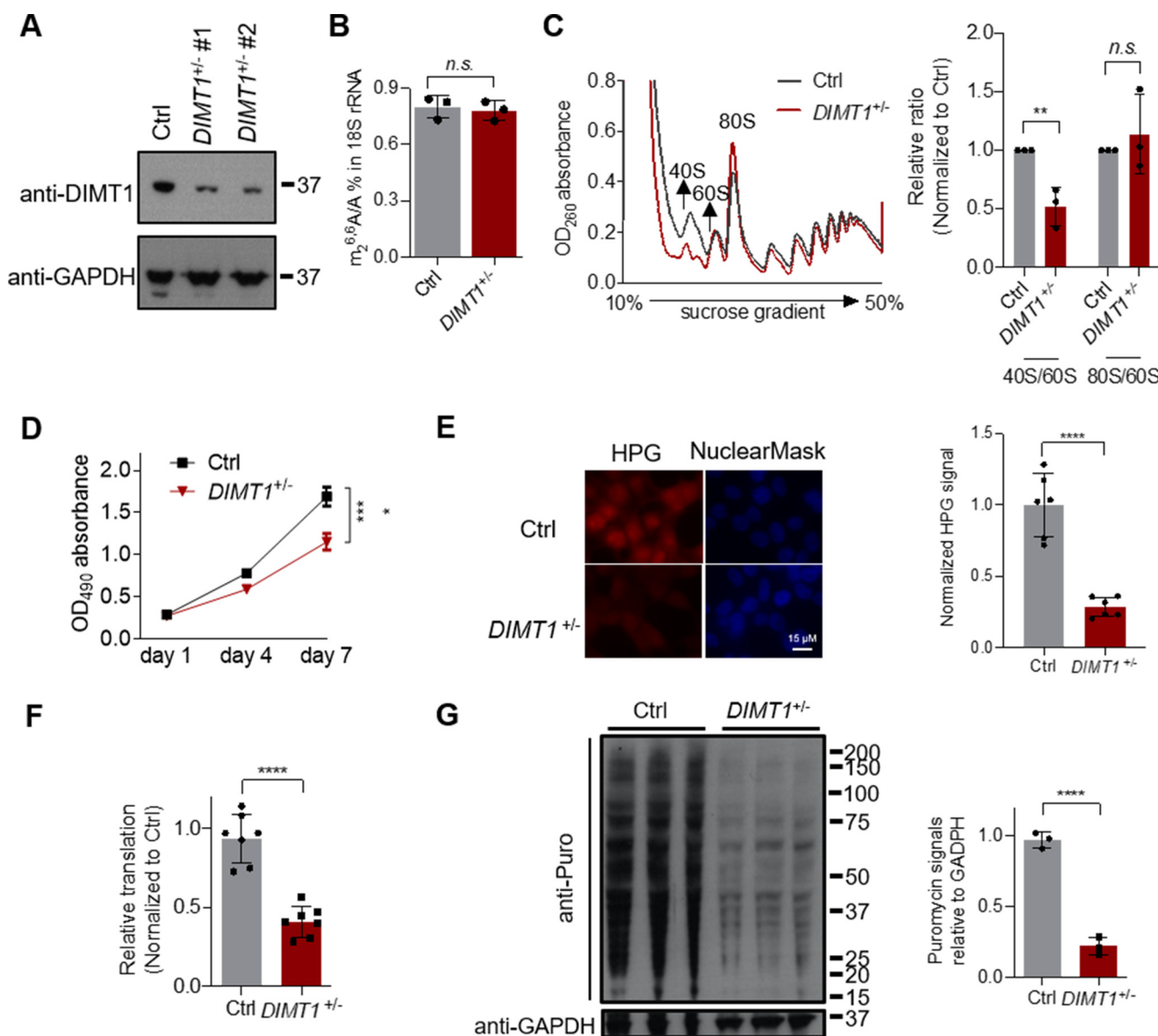


Figure 2. *DIMT1*^{+/-} leads to decreased 40S peak, protein synthesis, and cell proliferation. **A**, Western blotting of DIMT1 in WT and two *DIMT1*^{+/-} single colonies. **B**, LC-MS/MS quantification of m₂⁶A in 18S extracted from WT and *DIMT1*^{+/-} cells. **C**, polysome profiles of WT and *DIMT1*^{+/-} cells. The ratios of 40S to 60S and 60S to 80S were determined from two biological replicates (the second set is in Fig. S4C). **D**, cell proliferation assays performed in the WT and *DIMT1*^{+/-} cells. **E**, imaging and quantification of fluorescence-labeled HPG signals in WT and *DIMT1*^{+/-} cells. Nuclei were stained with NuclearMask. **F**, *in vitro* translation performed using cell extract from WT and *DIMT1*^{+/-} cells. **G**, Western blotting of puromycin in WT and *DIMT1*^{+/-} cells. The error bars show the integrated signals from each Western blotting sample in the image quantified by ImageJ. *p* values were determined using a two-tailed Student's *t* test for unpaired samples. Error bars represent mean ± S.D. **, *p* < 0.01; ****, *p* < 0.0001; n.s., not significant.

collectively show that the DIMT1 deficiency significantly impacts 40S assembly and global protein translation.

DIMT1 E85A is catalytically inactive

The catalytic activity of DIMT1 was suggested to not be required for 18S rRNA processing in yeast and human cells in a previous report (15, 17, 19, 26). To explore the catalytic role of DIMT1, we intended to first identify a catalytic-inactive DIMT1 variant. Thus, we performed protein sequence alignment (Fig. S4E) of DIMT1 in multiple species. Based on the sequence alignment and previous studies of DIMT1 in prokaryotes and yeast (19, 36), we selected Glu85 to mutate. An additional reason Glu85 was chosen for mutational analysis is that mutation at this

residue was shown in patients with glioblastoma multiforme (37). We cloned, expressed, and purified full-length recombinant human WT and E85A variant DIMT1 proteins (Fig. S4F). We then performed *in vitro* methylation assays using the DIMT1 E85A variant and WT DIMT1 with a synthetic RNA probe bearing the same local structure as the two m₂⁶A sites in the 18S rRNA 45 helix (Fig. 3A). The LC-MS/MS results showed that WT DIMT1 effectively installs m₂⁶A in this RNA probe (Fig. 3, A and B). In contrast, the E85A DIMT1 variant failed to install m₂⁶A in the RNA probe (Fig. 3, A and B and Fig. S5). Furthermore, we determined the structure of the E85A DIMT1 variant. Glu85 in WT DIMT1 and the mutated Ala85 in DIMT1 E85A are clearly modeled in the electron density map (Fig. 3C). The overall structures of WT DIMT1 and

Catalytic-dependent and -independent roles of human DIMT1

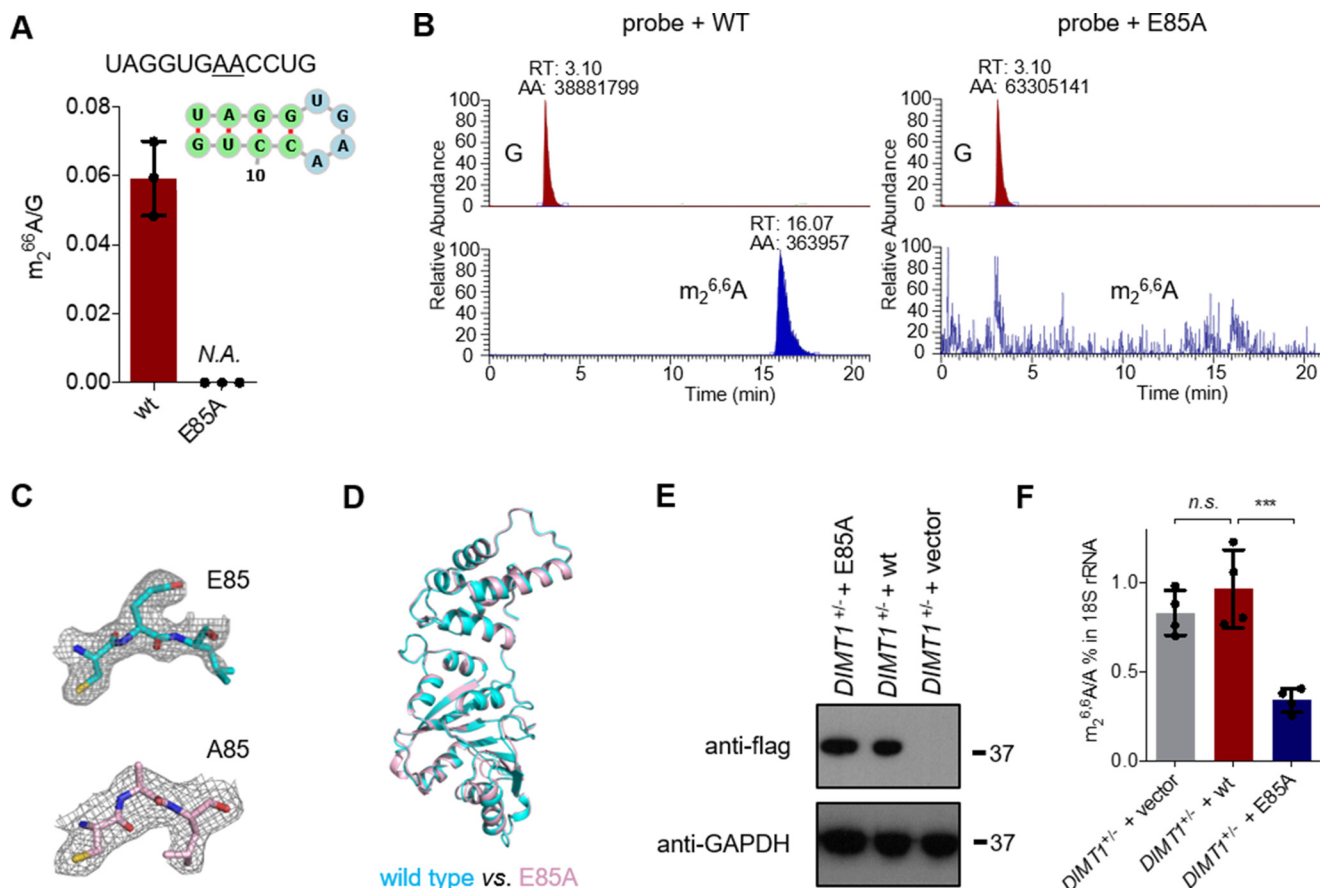


Figure 3. Identification of catalytically inactive E85A DIMT1 variant. A, LC-MS/MS quantification of $m_2^{6,6}A$ levels in an unmodified RNA probe after *in vitro* methylation reaction with WT or E85A DIMT1. SAM was supplemented in the *in vitro* methylation activity assay. B, LC-MS/MS channels and peak areas of guanosine and $m_2^{6,6}A$ in the *in vitro* reactions with WT or E85A DIMT1 variant. C, final $2F_o - F_c$ electron density maps of Glu85 in WT DIMT1 and Ala85 in E85A DIMT1 contoured at 1.0 σ and in gray. D, overlapped structures of WT and E85A DIMT1. E, Western blotting showing the expression of FLAG-tagged DIMT1 in DIMT1^{+/-} + E85A, DIMT1^{+/-} + WT (wt), and DIMT1^{+/-} + empty vector. F, LC-MS/MS quantification of $m_2^{6,6}A$ in 18S rRNA extracted from DIMT1^{+/-} + E85A, DIMT1^{+/-} + WT (wt), and DIMT1^{+/-} + empty vector. *p* values were determined using a two-tailed Student's *t* test for unpaired samples. Error bars represent mean \pm S.D. ***, *p* < 0.001; n.s., *p* > 0.05; N.A., not determined.

E58A are nearly identical; the superimposition of WT and E58A variant yields r.m.s.d. of 0.578 Å for 271 residues (Fig. 3D).

To measure the methyltransferase activity of E85A DIMT1 variant on 18S rRNA inside cells, we constructed cell lines stably expressing either FLAG-HA-tagged E58A, FLAG-HA-tagged WT DIMT1, or empty vector in our previously established DIMT1^{+/-} HEK 293T cells (Fig. 3E). As shown in Fig. 3F, the cells expressing E58A variant have a greatly decreased level of $m_2^{6,6}A$ in 18S rRNA compared with that of the cells expressing WT DIMT1. These results suggest that the expression of E58A DIMT1 leads to a dominant-negative effect in decreasing the level of $m_2^{6,6}A$ in 18S rRNA in DIMT1^{+/-} HEK 293T cells. Indeed, we observed a decreased level of $m_2^{6,6}A$ in 18S rRNA when we expressed the E85A DIMT1 variant in WT cells as well but to a lesser extent than expressing E85A DIMT1 variant in DIMT1^{+/-} heterozygotes cells (Fig. 3F and Fig. S6, A and B).

DIMT1 E85A variant does not have a major impact on 18S rRNA processing and ribosome assembly but impairs protein synthesis

We further studied the catalytic role of DIMT1 on 18S processing, ribosome assembly, and global protein synthesis. As shown in Fig. S7A, the E85A DIMT1 variant did not lead to

noticeable changes in the ratio of 18S to 28S rRNA. The results from qRT-PCR quantification of 18S rRNA extracted from WT and E85A DIMT1 variants are consistent with the results from the agarose gel images (Fig. S7, B and C). To analyze whether the DIMT1 E85A variant impairs 40S assembly, we conducted polysome profiling using cell lysate from DIMT1^{+/-} + WT, DIMT1^{+/-} + E85A, and DIMT1^{+/-} + empty vector cell lines. As shown in Fig. 4A and Fig. S7D, DIMT1^{+/-} + E85A variant cells did not show obvious changes in the polysome profiles compared with that of the DIMT1^{+/-} + WT cells, whereas DIMT1^{+/-} + empty vector showed a major decrease specifically in the 40S assembly. These results suggest that the protein scaffold but not the catalytic role of DIMT1 is required for ribosome assembly. We further carried out EMSA (electrophoretic mobility shift assay/gel shift assay) to compare the RNA binding affinity of WT and E85A DIMT1. As shown in Fig. S7, E and F, E85A only displays a slight decrease of affinity to the RNA probes (the same as that used in $m_2^{6,6}A$ LC-MS/MS quantification) compared to WT DIMT1. In contrast, both DIMT1^{+/-} + E85A variant cells and DIMT1^{+/-} + empty vector cells present decreased protein synthesis, whereas the DIMT1^{+/-} + WT cells showed protein synthesis comparable to that of the knockout control cells, as revealed in the HPG assays and the *in vitro* translation assays

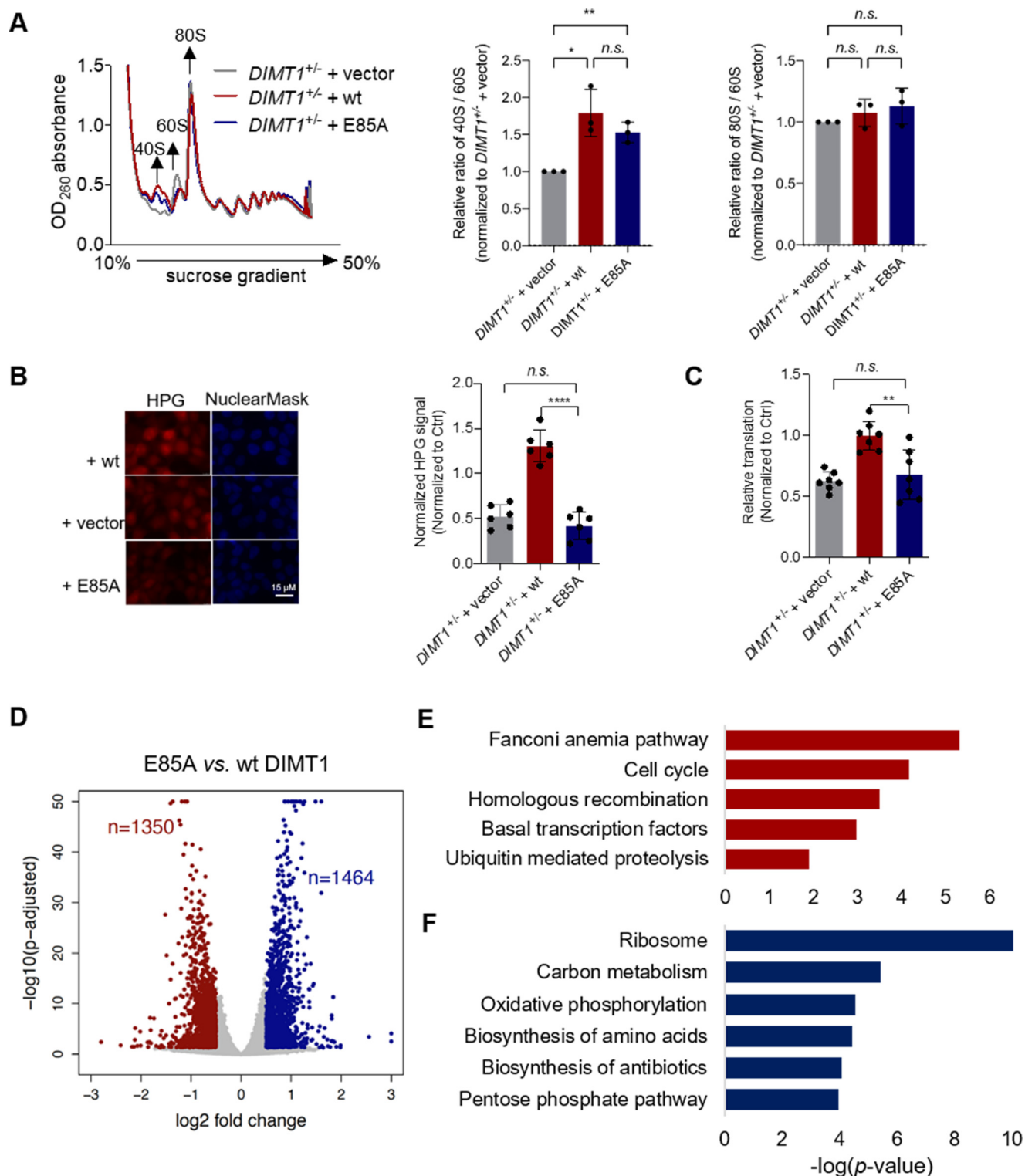


Figure 4. Catalytically inactive E85A DIMT1 leads to decreased 40S and impaired protein synthesis. *A*, polysome profiles of $DIMT1^{+/-}$ + E85A, $DIMT1^{+/-}$ + WT, and $DIMT1^{+/-}$ + empty vector cells. The ratios of 40S to 60S and 60S to 80S were determined from two biological replicates (the second set is in Fig. S7D). *B*, imaging and quantification of fluorescence-labeled HPG signals in $DIMT1^{+/-}$ + E85A, $DIMT1^{+/-}$ + WT, and $DIMT1^{+/-}$ + empty vector cells. Nuclei were stained with NuclearMask. *C*, *in vitro* translation performed using cell extract from $DIMT1^{+/-}$ + E85A, $DIMT1^{+/-}$ + WT, and $DIMT1^{+/-}$ + empty vector cells. The signals were normalized to the knockout control cells. *D*, volcano plots showing gene expression in $DIMT1^{+/-}$ + E85A and $DIMT1^{+/-}$ + WT cells. Differentially expressed genes are shown in red and blue (adjusted $p < 0.05$, \log_2 fold change of >0.5 , or \log_2 fold change of <-0.5). GO enrichment analysis of the downregulated (*E*) and upregulated (*F*) genes between $DIMT1^{+/-}$ + E85A and $DIMT1^{+/-}$ + WT cells. p values were determined using a two-tailed Student's t test for unpaired samples. Error bars represent mean \pm S.D. *, $p < 0.05$; **, $p < 0.01$; ***, $p < 0.0001$; n.s., $p > 0.05$.

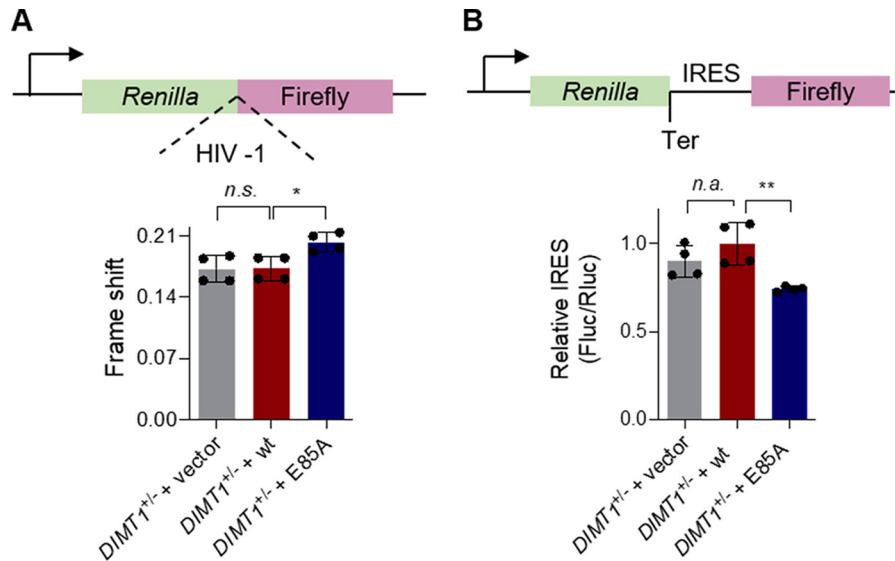


Figure 5. E85A DIMT1 leads to increased –1 frameshift and decreased IRES association. A, the E85A DIMT1 variant promotes –1 PRF. –1 PRF mediated by the HIV frameshift signal and without the insertion of HIV-1 signal were recorded from DIMT1^{+/-} + E85A, DIMT1^{+/-} + WT, and DIMT1^{+/-} + empty vector cells. B, EMCV IRES-dependent translation is inhibited in cells expressing the E85A DIMT1 mutant. EMCV IRES activity was measured using a Dual-Luciferase reporter using DIMT1^{+/-} + E85A, DIMT1^{+/-} + WT, and DIMT1^{+/-} + empty vector cells. *p* values were determined using a two-tailed Student's *t* test for unpaired samples. Error bars represent mean ± S.D. *, *p* < 0.05; **, *p* < 0.01; n.s., *p* > 0.05.

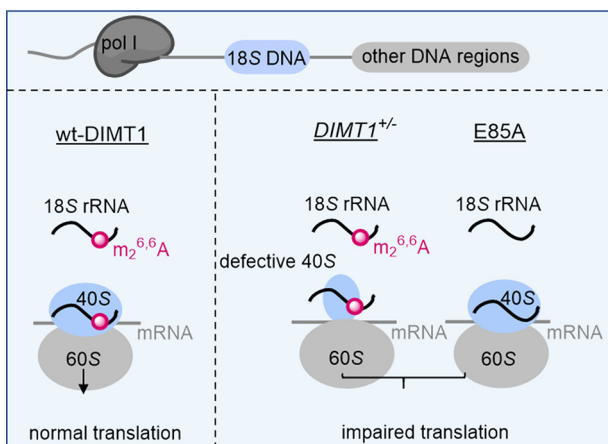


Figure 6. Schematic summary of the catalytic and structural roles of human DIMT1.

(Fig. 2, E and F, and 4, B and C). The HPG results obtained using WT cells expressing empty vector, E85A variant DIMT1, or WT DIMT1 are consistent with the results obtained from the cells with the DIMT1^{+/-} genetic background (Fig. S7G). These data have lent support to the conclusion that the catalytic role of DIMT1, although not required for 40S assembly, is important for protein translation.

The catalytic efficiency of human DIMT1 is important for the expression of genes involved in DNA damage response

To better understand the role of DIMT1 catalysis in gene regulation and cellular function, we performed RNA-seq with purified poly(A)-RNA from DIMT1^{+/-} + WT cells and +E85A variant cells. The biological replicates of the RNA-seq showed strong concordance between replicates, and the RNA-seq was validated by using qRT-PCR (Fig. S8, A and B). No enrichment for

nonspecific RNA fragments, such as rRNA fragments, was observed in the sequencing results. The RNA-seq identified 1464 coding genes that were upregulated (*p* < 0.05 and log₂ fold change of >0.5) and 1350 coding genes that were downregulated (*p* < 0.05 and log₂ fold change of <-0.5) in DIMT1 variant cell lines compared with the WT cell line (Fig. 4D). Gene ontology analysis of the upregulated genes in DIMT1 variant cell lines revealed a strong enrichment for DNA damage repair and cell cycle arrest (Fig. 4E). The downregulated genes revealed a strong enrichment for energy metabolism regulation, which is expected because DIMT1 is a ribosome assembly factor and important for ribosome functions (Fig. 4F).

Defects in 18S rRNA m_{2,6}A impair internal ribosomal entry site (IRES)-dependent translation and translation fidelity in mammalian cells

One important function of the ribosome is to faithfully maintain the translational reading frame. In this process, *cis*-acting mRNA elements (–1 PRF signals) direct translating ribosomes to slip on an mRNA by one base in the 5' direction, thereby establishing a new reading frame (30). Viral mRNA signals that abrogate this function by programming ribosomes to shift frames (programmed ribosomal frameshifting, or PRF) have proven to be of tremendous utility as readouts of translation fidelity (38). This phenomenon has been previously reported in mammalian cells, especially under ribosomal defects and disease conditions. As shown in Fig. S1, DIMT1-mediated m_{2,6}A sites in 18S rRNA are at the interface between 40S and 60S subunits. These sites have contacts with both mRNA and tRNA on the ribosome and may be important for preventing frameshifting. Thus, to study whether DIMT1-mediated m_{2,6}A is important for preventing frameshift, we used Dual-Luciferase reporters to quantify changes in PRF signals guided by the HIV-1 PRF. As shown in Fig. 5A, DIMT1^{+/-} + E85A variant DIMT1 promotes a

30% increase of -1 PRF compared with *DIMT1*^{+/-} + WT cells and + empty vector cells, which both show no change of m₂^{6,6}A levels in 18S rRNA (Fig. 3F). Thus, the results suggest that DIMT1-mediated m₂^{6,6}A sites in 18S rRNA participate in the regulation of translation fidelity in mammalian cells, which is consistent with the previous findings that Dim1 inactivation produces fidelity defects in yeast (39).

Furthermore, it has been reported that defects in rRNA modifications affect IRES-dependent translation (30). To investigate whether m₂^{6,6}A sites in 18S rRNA impact IRES association, we employed an encephalomyocarditis virus (EMCV) IRES reporter (40) to investigate whether DIMT1-mediated m₂^{6,6}A in 18S rRNA plays a role in ribosome association with IRES sequences. The EMCV IRES directly binds the eIF4G subunit of the eIF4 complex and bypasses the requirement of the cap and cap-binding factor eIF4E. We transfected the EMCV IRES reporters in *DIMT1*^{+/-} + WT, + E85A variant DIMT1, or + empty vector cell lines. As shown in Fig. 5B, only cells expressing the E85A variant but not cells expressing empty vector present decreased luciferase signals. Of note, E85A-expressing cells but not empty vector-expressing cells show decreased levels of m₂^{6,6}A in 18S rRNAs. Instead of using *DIMT1*^{+/-} cells, WT HEK 293T cells + E85A variant DIMT1, but not cells expressing empty vector, showed decreased luciferase signals (Fig. S9A). In addition, we obtained similar results in cells under transient knockdown of DIMT1 compared with the knockdown control (Fig. S9B). Thus, these results suggest that DIMT1-mediated 18S m₂^{6,6}A can influence ribosome association with the EMCV IRES sequence.

Discussion

Previous studies have suggested the overall scaffold of DIMT1 is important for 18S processing and ribosome assembly. However, the function of DIMT1-mediated m₂^{6,6}A in 18S rRNA remains elusive. In this work, we show that lack of such a catalytic activity of human DIMT1 significantly decreases protein synthesis and translation fidelity, although this catalytic role of DIMT1 is not required for ribosome small subunit assembly. We found that DIMT1 ablation impairs 40S assembly and global translation. Furthermore, we have also studied the biological significance of the overall protein scaffold of DIMT1, including both the catalytic and noncatalytic domains, in ribosome assembly and translation. We also identified and characterized a catalytically inactive DIMT1 variant E85A that has a dominant-negative effect on decreasing m₂^{6,6}A levels in 18S rRNA. Of note, expressing E85A DIMT1 leads to significantly decreased 40S assembly and global protein synthesis. These results, together with those of previous studies, support a model in which DIMT1 has a structural role in 18S rRNA processing and ribosome biogenesis and a catalytic role in protein synthesis and the regulation of translation fidelity, conferring a more comprehensive picture (Fig. 6).

Because previous studies show the high prevalence and progressively increased levels of DIMT1 in myeloma and acute leukemia (22, 23), small molecules inhibiting DIMT1 catalytic efficiencies should be pursued. DIMT1-mediated m₂^{6,6}A dimethylation sites are in the interface between the 40S and

60S ribosomes, which makes these sites accessible to the small-molecule inhibitors. We determined the crystal structures of WT DIMT1 that will facilitate rational inhibitor design. There is a deposited but not published structure of human DIMT1 in complex with SAH (PDB entry 1ZQ9). The ligand-free structure of human DIMT1 solved in this study superimposed well with the cofactor-bound structure (Fig. S10), which suggests that binding SAH does not cause major structural changes of DIMT1. Furthermore, we solved the structure of a catalytically inactive variant E85A DIMT1, which shows no major structural changes from WT DIMT1. E85G mutation of DIMT1 was frequently seen in patients with colon adenocarcinoma (41). We predicted that the mutation at the Glu85 site (either E85A or E85G) also slightly impairs the stability of the protein using bioinformatic algorithms (42). These studies suggest the catalytic residues of DIMT1 may contribute to the pathological mechanism.

The finding of the biologic consequence of m₂^{6,6}A modifications in 18S rRNA by DIMT1 is important and potentially inspiring, because there are several other similar rRNA-modifying enzymes (e.g. Emg1/EMG1 and Bud23/WBSCR22) that are suggested to function as a scaffold in preribosomal complexes, and whether their catalytic activities are not required for pre-rRNA processing is still unknown (14, 28). Given that most of the mechanistic studies were carried out in prokaryotes and yeast, our understanding of the molecular functions of rRNA modifications in mammals is limited. Thus, the study of these rRNA-modifying enzymes and their functions will likely reveal previously uncharacterized regulatory mechanisms.

The rRNA species are extensively modified. The downstream effects of most of the modifications remain elusive. DIMT1-mediated m₂^{6,6}A dimethylation in the two adjacent sites in 18S rRNA is conserved from prokaryote to mammals. However, only the structural role of DIMT1 was thought to be important for 18S rRNA processing and ribosome assembly in yeast. One previous study carried out in human cells using siRNA to transiently knock down DIMT1 drew essentially the same conclusion that the catalytic role of DIMT1 is nonessential (19). The *t*_{1/2} of rRNAs range from 3–8 days among different human cell lines (43). Notably, we constructed stable cell lines expressing DIMT1 inactive variants that have a dominant-negative effect in decreasing the level of m₂^{6,6}A in 18S rRNA. Our system removes the possibility that the nondecayed 18S rRNA still functions. Our results are consistent with the previous discoveries and suggest that the catalytic-inactive DIMT1 variants do not alter 18S rRNA processing. However, the catalytic-inactive DIMT1 variants showed significant defects in 40S assembly and global protein synthesis. Further analyses revealed a previously uncharacterized function of the catalytic role of DIMT1 in the regulation of IRES association, translation fidelity, and the expression of genes involved in DNA repair. The expression of the catalytically inactive E85A variant DIMT1 leads to a modest decrease of EMCV IRES signals compared with the cells expressing WT DIMT1; however, this modest change cannot fully explain the drastic defects in protein synthesis. The transcriptional change shown in the RNA-seq data and other factors may also contribute to the difference in protein synthesis between E85A- and WT DIMT1-expressing cells.

Catalytic-dependent and -independent roles of human DIMIT1

In summary, this study began to uncover both the catalytic, *i.e.* m²_{6,6}A in 18S rRNA, and noncatalytic biological consequences of human DIMIT1. The results highlighted the significant impact of DIMIT1 on ribosomal small subunit assembly and translation. It is possible that DIMIT1 possesses other undiscovered activities that need to be further investigated in future studies. Ribosome assembly and translation are complex processes involving many components and regulated by many factors. The findings described in this report will open a new avenue to study these critical biological processes.

Materials and methods

Construction, expression, and purification

Human *DIMIT1* gene (gene ID 27292) was cloned from a human cDNA library and ligated into pET-28a vector for protein expression, and pPB vector was used for overexpression in mammalian cells. On the basis of this WT plasmid, the E85A mutant was constructed using fusion PCR and validated by Sanger sequencing. The primers used are listed in Table S2. pET-28a plasmids were transformed into *Escherichia coli* BL21(DE3) for purification. Expression of all recombinant proteins was induced with 0.5 mM IPTG when the cell density reached an optical density at 600 nm between 0.6 and 0.8. After growth for ~20 h at 16 °C, the cells were collected and lysed in the lysis buffer (25 mM Tris, pH 7.5, 500 mM NaCl). After centrifugation at 4 °C for 30 min, the supernatant was loaded onto a Ni²⁺-affinity chromatography column (GE Healthcare), which was preequilibrated using the lysis buffer. The column then was washed three times with wash buffer (50 mM imidazole in lysis buffer), and the bound target protein was eluted with elution buffer (500 mM imidazole in lysis buffer). The eluted proteins were further purified with a HiTrap SPFF (GE Healthcare) column using a gradient elution formed by low-salt buffer (25 mM Tris, pH 7.5, 50 mM NaCl) and high-salt buffer (25 mM Tris, pH 7.5, 1 M NaCl) and a HiLoad Superdex 200 (GE Healthcare) column with S200 buffer (25 mM Tris, pH 7.5, 200 mM NaCl).

Crystallization, data collection, and structure determination

Crystals of both the WT and E85A mutant DIMIT1 were grown at 12 mg/ml using the hanging-drop vapor diffusion method at 290 K and grew to maximum size in ~1 day in the buffer containing 0.2 M ammonium sulfate, 0.1 M Tris-HCl, pH 8.5, 20% PEG 3350. Crystals were transferred to cryoprotectant solution consisting of the respective reservoir solution supplemented with 25% (v/v) glycerol and then flash-cooled in liquid nitrogen. Data sets for all crystals were collected at the ID-17 beamline of the National Synchrotron Light Source II (NSLS-II) of the Brookhaven National Laboratory at a wavelength of 0.920 Å and at 100 K. The data sets were processed and scaled with HKL-3000. The structures were determined by the molecular-replacement method using MOLREP (44) as implemented in the CCP4 (45) package. All of the initial models were refined using the maximum-likelihood method implemented in REFMAC5 (46) as part of the CCP4 program suite and rebuilt interactively using Coot (47). The final models were evaluated with MolProbity (48) and PROCHECK (49). The crystallographic parameters are listed in Table S1. The structure figures shown in this work were

prepared with PyMOL. For the structures of WT and E85A DIMIT1, the resolution cutoff was decided based on the mean $I/\sigma(I)$ of the highest-resolution shell of >2 and an overall R_{merge} of <20%.

In vitro methylation assay

The *in vitro* methylation assays were performed in a 30-μl reaction mixture containing the following components: 4 μg biotinylated RNA probes, 24 μg protein (WT DIMIT1 or E85A mutant), 1 mM SAM, 50 mM Tris, pH 7.5, 5 mM MgCl₂, and 1 mM DTT. The reaction mixture was incubated at 16 °C overnight. After incubation, streptavidin beads (Thermo Scientific) were used to purify the RNA probes, following the instructions from the manufacturer, and eluted with RNase-free water at 75 °C for 5 min. The purified RNA probes then were digested and dephosphorylated to single nucleosides using nucleoside digestion mix (NEB, M0649S) for LC-MS/MS quantification. The sequence of the RNA probe is listed in Table S2.

EMSA

The RNA probe was purchased from IDT with the sequence of 5'-rUrUrCrCrGrUrArGrGrUrGrArArCrCrUrGrCrGrGrArA-3', which stemmed from human 18S rRNA sequence. The RNA probe was dissolved by RNase-free water at 4 mM and diluted to 40 μM in EMSA binding buffer (25 mM Tris, pH 7.2, 150 mM NaCl, and 40 U/ml RNasin). The RNA probe then was heated at 75 °C for 5 min to denature it. WT and E85A DIMIT1 were diluted to a concentration series of 5 μM, 10 μM, 20 μM, 40 μM, and 80 μM in EMSA assay binding buffer. 1 μl RNA probe and 1 μl protein were mixed with 3 μl binding buffer, and the mixture was incubated on ice for 30 min. The entire 5-μl RNA-protein mixture was loaded to the 10% TBE gel with 1 μl loading buffer (1% bromophenol blue and 50% glycerol) and then subjected to electrophoresis for 50 min at 120 V in a 4 °C cold room. The gel was stained by SYBR Gold (Invitrogen, S11494) at room temperature for 5 min. Quantification was carried out using ImageJ to quantify intensity of the bottom free RNA band. The K_D (dissociation constant) was calculated with nonlinear curve fitting (function Hyperbl) of Origin 8 software with $y = (P1 \times x)/(P2 + x)$, where y is the ratio of [RNA-protein]/[total RNA], x is the concentration of the protein, $P1$ is set to 1, and $P2$ is K_D .

Mammalian cell culture, siRNA knockdown, and plasmid transfection

HEK 293T cells were cultured in Dulbecco's modified Eagle medium (GIBCO, 11995065) supplemented with 10% FBS (GIBCO, 26140-079) and 1% penicillin-streptomycin (Corning, 30-002-CI) in a 37 °C, 5% CO₂ incubator. Negative-control siRNA from Ambion (AM4611) was used as a control siRNA in the knockdown experiments. *DIMIT1* siRNA was purchased from Ambion (AM16708). Lipofectamine 2000 (11668019) and Lipofectamine RNAiMax (13778150), from Invitrogen, were used for plasmid and siRNA transfection, respectively, by following the manufacturer's instructions. It took 48 h for siRNA knockdown and 24 h for plasmid overexpression.

Quantitative analysis of the $m_2^{6,6}A$ level using LC-MS/MS

For transient knockdown, cells were seeded in 6-well plate at 40% confluence, and 2 μ l of 20 nM siDIMT1 or control RNA was transfected to each corresponding well using Lipofectamine RNAiMax by following the manufacturer's instructions on the next morning. After 48 h of culturing in a 37°C, 5% CO₂ incubator, cells were collected with cell lifter and the 18S RNA was extracted as indicated in the RNA isolation section below. Purified RNA or RNA probes were digested and dephosphorylated to single nucleosides using nucleoside digestion mix (NEB, M0649S) at 37°C for 1 h. The detailed procedure was as previously described (50). The nucleosides were quantified using retention time and nucleoside-to-base ion mass transitions of 268.0→136.0 (A), 284.0→152.0 (G), and 296.0→164.1 ($m_2^{6,6}A$). All quantifications were performed by converting the peak area from the LC-MS/MS to moles using the standard curve obtained from pure nucleoside standards. The percentage ratio of $m_2^{6,6}A$ to G then was used to compare the different modification levels.

Construction of knockout cell lines using CRISPR

Two pairs of single guide RNAs (sgRNAs) for *DIMT1* were designed by using a website tool. These sgRNAs were then individually cloned into a pX459 vector (51). The plasmids containing these sgRNAs were subsequently transfected to HEK 293T cells using Lipofectamine 2000 (Invitrogen). After 24 h, 2 μ g/ml puromycin was administered for another 48 h. The surviving cells were cultured as single colonies into 96-well plates to screen for the positive *DIMT1* monoclonal knockout. 2 weeks later, single colonies were screened by PCR. Further validation was conducted using Western blotting with an antibody from Abcam (ab184978) and Sanger sequencing. The colonies showing as WT *DIMT1* in Sanger sequencing are considered control knockout cells. The sequences of sgRNAs and primers employed used in the PCR screening are listed in Table S2.

Construction of stable overexpression cell lines

FLAG-HA-tagged WT *DIMT1*, FLAG-HA-tagged E85A mutant, or empty overexpression vector (pPB backbone) were transfected into WT HEK 293T cells or *DIMT1*^{+/-} heterozygous HEK 293T cells. The cells were selected under 2 μ g/ml puromycin for 2 weeks. During the selection period, cells were resuspended every 2 days with fresh DMEM supplemented with 10% FBS and 2 μ g/ml puromycin. After 7 days, the surviving cells were separated into single cells in a 96-well plate and subjected to puromycin selection for another 7 days. The stable overexpression was confirmed by Western blotting using an anti-FLAG antibody (Thermo, MA1-91878-HRP).

Cell proliferation assay

The cells were first trypsinized and counted using a cell counting chamber slide (Invitrogen, 100078809). 1000 cells then were seeded into every well in a 96-well plate in 100 μ l cell culture medium. The next day, 20 μ l of CellTiter 96® Aqueous One solution (Promega) was added to each well at 37°C, 5% CO₂ for 2 h. Absorbance at 490 nm was then measured using a GloMax plate reader (Promega).

Polysome profiling

Cells were seeded in a 10-cm plate 1 day before at 70% confluence. Before collecting cells, cycloheximide (CHX) was added to the cell culture medium at 100 μ g/ml for 7 min. The medium then was discarded, and the cells were washed once with ice-cold 1× PBS containing CHX (100 μ g/ml). The cells were collected by a cell lifter with 5 ml cold PBS containing CHX (100 μ g/ml). Cells were pelleted at 500 × *g* for 3 min at 4°C and resuspended with 500 μ l lysis buffer (10 mM Tris, pH 7.4, 150 mM KCl, 5 mM MgCl₂, 100 μ g/ml CHX, 0.5% Triton-X-100, freshly added protease inhibitor, 40 U/ml SUPERasin). After lysing on ice for 15 min, the supernatant was collected by centrifugation at 15,000 × *g* for 15 min. The cell lysate was then layered on top of a linear 10–50% sucrose gradient (10 mM Tris, pH 7.4, 150 mM KCl, 5 mM MgCl₂, 100 μ g/ml CHX, 40 U/ml SUPERasin) and centrifuged at 4°C for 150 min at 35,000 rpm (Beckman, rotor SW-40Ti). The samples then were fractionated and analyzed by a Gradient Station (BioCamp) equipped with a TRIAX flow cell (BioCamp). The ratios of the 40S peak to 60S peak and 80S peak to 60S peak were calculated for each polysome profile. These ratios were normalized to knockout control cells for *DIMT1*^{+/-} cells (Fig. 2C and Fig. S4C) or normalized to *DIMT1*^{+/-} + vector for *DIMT1*^{+/-} + wt and *DIMT1*^{+/-} + E85A (Fig. 4A and Fig. S7D) to remove batch effect for each experiment.

HPG assay

The HPG assay was performed using the Click-iT HPG Alexa Fluor 594 protein synthesis assay kits (Life Technologies, C10429) by following the manufacturer's instructions. Briefly, cells were cultured in 6-well plates, with one coverslip in each well. On the day of the experiment, the regular cell culture medium was replaced by 1 ml of L-methionine-free RPMI 1640 medium containing 1 μ l Click-iT reagent for 45 min. The cells then were washed once with 1×PBS and fixed with 3.6% formaldehyde in 1×PBS at room temperature for 15 min. After washing twice with 3% BSA, the cells were permeabilized using 0.5% Triton X-100 at room temperature for 20 min. The Click-iT reaction was carried out at room temperature for 30 min, followed by a quenching step. The DNA then was stained by HCS NuclearMask blue stain reagent for 3 min. Finally, the coverslips were mounted with antifade reagent (Invitrogen, P36970), and the images were captured using a Leica DM6000 motorized upright microscope with the same settings for all the images (Alexa Fluor 594 exposure time for all images was 500 ms, and NuclearMask Blue exposure time for all images was 2.5 ms). For quantification, six cells were unbiasedly selected in each HPG figure to intensify quantification of the integrated area using ImageJ. The regions next to the cells without fluorescence were similarly selected and quantified as the background. The following formula then was used to calculate the corrected cell fluorescence intensity: integrated intensity – (area of selected cell × mean integrated intensity of backgrounds). Finally, the fluorescence intensities of *DIMT1*^{+/-}, *DIMT1*^{+/-} + wt, *DIMT1*^{+/-} + vector, and *DIMT1*^{+/-} + E85A cells were all normalized to the one in knockout control cells.

Catalytic-dependent and -independent roles of human DIMT1

In vitro translation assay

In vitro translation was performed using a previously described protocol (35). Briefly, cells were seeded in a 10-cm plate at 70% confluence 1 day before, and cells were then trypsinized and collected by centrifugation for 5 min at $1,000 \times g$ at 4°C and washed once with ice-cold $1 \times$ PBS. The cells then were resuspended with an equal volume of freshly made ice-cold lysis buffer [10 mM HEPES-KOH, pH 7.6, 10 mM KOAc, 0.5 mM Mg(OAc)₂, 5 mM DTT, and 1 tablet of complete EDTA-free proteinase inhibitor mixture (Roche) per 10 ml of buffer]. After hypotonic-induced swelling for 45 min on ice, cells were homogenized by forcing the cell suspension through a 27-G needle about 10–15 times until ~95% of cells burst. The cell lysate was centrifuged at $14,000 \times g$ for 1 min at 4°C, and the supernatant was collected. The protein concentration in the extract was measured using a Bradford assay. An equal amount of cell lysate was used in the *in vitro* translation assays. Each translation reaction contained 50% cell lysate, 0.84 mM ATP, 0.21 mM GTP, 21 mM creatine phosphate (Roche), 45 U/ml creatine phosphokinase (Roche), 10 mM HEPES-KOH, pH 7.6, 2 mM DTT, 2 mM Mg(OAc)₂, 50 mM KOAc, 8 μM amino acids (Promega), 255 μM spermidine, and 1 U/μl RNase inhibitor. Translation reaction mixtures were incubated for 90 min at 30°C, after which luciferase activity was measured using a Dual-Luciferase reporter assay (Promega) with a GloMax plate reader (Promega). All measurements were normalized to the knockout control cells.

Protein quantitation and Western blotting

Protein concentration for samples was calculated using the Bradford assay (5000006, Bio-Rad). Protein samples were boiled at 95°C with Laemmli sample buffer for 10 min. After brief centrifugation, samples were loaded onto SDS-PAGE gels. After running at 180 V for 1 h, the gel was transferred to PVDF membranes by semidry transfer apparatus at 20 V for 50 min. The PVDF membranes then were blocked with 5% milk in $1 \times$ PBST for 30 min at room temperature and incubated with 3% milk in $1 \times$ PBST containing the corresponding antibody overnight at 4°C. After washing three times with $1 \times$ PBST, horseradish peroxidase (HRP)-conjugated secondary antibody (1:20,000) in 1% milk was applied and incubated at room temperature for 1 h. After washing three times with $1 \times$ PBST, the membrane was visualized using an ECL Western blotting detection kit (Thermo Fisher).

Protein synthesis assay

The rate of global protein synthesis was determined using puromycin to label nascent peptides as described previously (52). Briefly, cells were split into a 6-well plate 1 day before the experiment. After culturing overnight, 1 μM puromycin was added to the medium for 1 h. The cells then were washed twice with $1 \times$ PBS and collected using a cell lifter. Samples were then analyzed by SDS-PAGE followed by Western blotting using an anti-puromycin antibody (Sigma-Aldrich, MABE343). The intensity for each sample was quantified by ImageJ and normalized by the intensity of GAPDH as the loading control. The final signals were normalized to the control.

Dual-Luciferase reporter assay

For testing translation fidelity, we constructed an in-frame control, encoding a *Renilla*-firefly luciferase fusion protein, and a 5′–1-reading-frame reporter, with HIV 5′–1 frameshift signal (listed in Table S2) between *Renilla* and firefly luciferases. 5′–1 frameshift percentages are calculated by calculating the ratio of firefly to *Renilla* luciferase reads and then normalized to the in-frame control.

For IRES reporter assay, EMCV IRES Dual-Luciferase reporter (30) was used. Cells were split into a 6-well plate 1 day before, and then 1 μg reporter plasmid was used to transfect cells. 24 h later, the Dual-Luciferase reporter assay system kit (Promega) was used to examine the expression of the luciferases. The relative luciferase activity was calculated by dividing Fluc by Rluc and normalized to the individual control.

RNA isolation

For total RNA extraction, TRIzol reagent (Invitrogen) was used by following the manufacturer's instructions. For 18S rRNA, 5 μg total RNA was subjected to further separation on a 1.5% agarose gel. 18S rRNA in the gel slices were then extracted using a Zymoclean gel RNA recovery kit (R1011). Poly(A)-RNA was extracted from the total RNA by using a Dynabeads mRNA purification kit (Ambion) by following the manufacturer's instructions.

RNA-seq

Purified poly(A)-RNA was fragmented by sonication at 30 s on and 30 s off per cycle, for 30 cycles, using a Bioruptor Pico (Diagenode). The RNA-seq library then was constructed using a TruSeq stranded mRNA kit (Illumina). The samples were sequenced by Illumina NextSeq 550 with single-end 75-bp read length. Raw reads were mapped to the reference genome (hg38) using Hisat2 (53). Parameters used were –no-unal (not report the unaligned reads), –known-splicesite-file (generated from the UCSC hg38 annotation file), and –k 1 (report one alignment). Afterward, genomic alignments were counted in R using the GenomicAlignments package (54). Gene expression levels were normalized using DESeq2 (55). A significance threshold of adjusted *p* value of <0.05 was classified as statistically significant differential expression. Gene ontology analysis was carried out with the Database for Annotation Visualization and Integrated Discovery (DAVID) tool (56, 57).

Data availability

The sequence data have been deposited in the NCBI GEO database under the accession code GSE152811. All other data are available in the online Supporting Information. Atomic coordinates and structure factors for the reported crystal structures have been deposited with the Protein Data bank under accession numbers 6W6C and 6W6F.

Author contributions—H. S. data curation; H. S. and J. S. validation; H. S. and K. F. L. investigation; H. S. and K. F. L. writing-original draft; J. S. writing-review and editing; K. F. L. conceptualization; K. F. L. supervision; K. F. L. funding acquisition.

Funding and additional information—This work was supported by the National Institutes of Health (NIH) R35 to K. F. L. (GM133721). The content is solely the responsibility of the authors and does not necessarily represent the official views of the National Institutes of Health.

Conflict of interest—The authors declare that they have no conflicts of interest with the contents of this article.

Abbreviations—The abbreviations used are: NTD, N-terminal domain; CTD, C-terminal domain; r.m.s.d., root mean square deviation; IRES, internal ribosomal entry site; PRF, programmed ribosomal frameshifting; EMCV, encephalomyocarditis virus; EMSA, electrophoretic mobility shift assay; sgRNAs, single guide RNAs; CHX, cycloheximide; HPG, homopropargylglycine.

References

- Strunk, B. S., Loucks, C. R., Su, M., Vashisth, H., Cheng, S., Schilling, J., Brooks, C. L., 3rd, Karbstein, K., and Skiniotis, G. (2011) Ribosome assembly factors prevent premature translation initiation by 40S assembly intermediates. *Science* **333**, 1449–1453 [CrossRef Medline](#)
- Pena, C., Hurt, E., and Panse, V. G. (2017) Eukaryotic ribosome assembly, transport and quality control. *Nat. Struct. Mol. Biol.* **24**, 689–699 [CrossRef Medline](#)
- Klinge, S., and Woolford, J. L. (2019) Ribosome assembly coming into focus. *Nat. Rev. Mol. Cell Biol.* **20**, 116–131 [CrossRef Medline](#)
- Natchiar, S. K., Myasnikov, A. G., Kratzat, H., Hazemann, I., and Klaholz, B. P. (2017) Visualization of chemical modifications in the human 80S ribosome structure. *Nature* **551**, 472–477 [CrossRef Medline](#)
- Polikanov, Y. S., Melnikov, S. V., Soll, D., and Steitz, T. A. (2015) Structural insights into the role of rRNA modifications in protein synthesis and ribosome assembly. *Nat. Struct. Mol. Biol.* **22**, 342–344 [CrossRef Medline](#)
- Chaker-Margot, M., Hunziker, M., Barandun, J., Dill, B. D., and Klinge, S. (2015) Stage-specific assembly events of the 6-MDa small-subunit processome initiate eukaryotic ribosome biogenesis. *Nat. Struct. Mol. Biol.* **22**, 920–923 [CrossRef Medline](#)
- Chaker-Margot, M., Barandun, J., Hunziker, M., and Klinge, S. (2017) Architecture of the yeast small subunit processome. *Science* **355**, eaal1880 [CrossRef](#)
- Poldermans, B., Bakker, H., and Van Knippenberg, P. H. (1980) Studies on the function of two adjacent N⁶,N⁶-dimethyladenosines near the 3' end of 16S ribosomal RNA of Escherichia coli. IV. The effect of the methylgroups on ribosomal subunit interaction. *Nucleic Acids Res.* **8**, 143–151 [CrossRef Medline](#)
- O'Farrell, H. C., Scarsdale, J. N., and Rife, J. P. (2004) Crystal structure of KsgA, a universally conserved rRNA adenine dimethyltransferase in Escherichia coli. *J. Mol. Biol.* **339**, 337–353 [CrossRef Medline](#)
- Mangat, C. S., and Brown, E. D. (2008) Ribosome biogenesis; the KsgA protein throws a methyl-mediated switch in ribosome assembly. *Mol. Microbiol.* **70**, 1051–1053 [CrossRef Medline](#)
- Tu, C., Tropea, J. E., Austin, B. P., Court, D. L., Waugh, D. S., and Ji, X. H. (2009) Structural basis for binding of RNA and cofactor by a KsgA methyltransferase. *Structure* **17**, 374–385 [CrossRef Medline](#)
- Boehringer, D., O'Farrell, H. C., Rife, J. P., and Ban, N. N. (2012) Structural insights into methyltransferase KsgA function in 30S ribosomal subunit biogenesis. *J. Biol. Chem.* **287**, 10453–10459 [CrossRef Medline](#)
- Poldermans, B., Roza, L., and Van Knippenberg, P. H. (1979) Studies on the function of two adjacent N⁶,N⁶-dimethyladenosines near the 3' end of 16 S ribosomal RNA of Escherichia coli. III. Purification and properties of the methylating enzyme and methylase-30S interactions. *J. Biol. Chem.* **254**, 9094–9100 [Medline](#)
- Sloan, K. E., Warda, A. S., Sharma, S., Entian, K. D., Lafontaine, D. L. J., and Bohnsack, M. T. (2017) Tuning the ribosome: the influence of rRNA modification on eukaryotic ribosome biogenesis and function. *RNA Biol.* **14**, 1138–1152 [CrossRef Medline](#)
- Johnson, M. C., Ghalei, H., Duxtader, K. A., Karbstein, K., and Stroupe, M. E. (2017) Structural heterogeneity in pre-40S ribosomes. *Structure* **25**, 329–340 [CrossRef Medline](#)
- Lafontaine, D., Delcour, J., Glasser, A. L., Desgres, J., and Vandenhaute, J. (1994) The Dim1 gene responsible for the conserved M(2)(6)Am(2)(6)a dimethylation in the 3'-terminal loop of 18-S ribosomal-RNA is essential in yeast. *J. Mol. Biol.* **241**, 492–497 [CrossRef Medline](#)
- Tokuhi, J. G., Vijayan, P., Feldmann, K. A., and Browse, J. A. (1998) Chloroplast development at low temperatures requires a homolog of DIM1, a yeast gene encoding the 18S rRNA dimethylase. *Plant Cell* **10**, 699–711 [CrossRef Medline](#)
- Wieckowski, Y., and Schiefelbein, J. (2012) Nuclear ribosome biogenesis mediated by the DIM1A rRNA dimethylase is required for organized root growth and epidermal patterning in Arabidopsis. *Plant Cell* **24**, 2839–2856 [CrossRef Medline](#)
- Zorbas, C., Nicolas, E., Wacheul, L., Huvelle, E., Heurgue-Hamard, V., and Lafontaine, D. L. J. (2015) The human 18S rRNA base methyltransferases DIMT1L and WBSR22-TRMT112 but not rRNA modification are required for ribosome biogenesis. *Mol. Biol. Cell* **26**, 2080–2095 [CrossRef Medline](#)
- Zou, J., Zhang, W., Zhang, H., Zhang, X. D., Peng, B., and Zheng, J. (2018) Studies on aminoglycoside susceptibility identify a novel function of KsgA to secure translational fidelity during antibiotic stress. *Antimicrob. Agents Chemother.* **62**, e00853-18 [CrossRef](#)
- Kiga, K., Mimuro, H., Suzuki, M., Shinozaki-Ushiku, A., Kobayashi, T., Sanada, T., Kim, M., Ogawa, M., Iwasaki, Y. W., Kayo, H., Fukuda-Yuzawa, Y., Yashiro, M., Fukayama, M., Fukao, T., and Sasakawa, C. (2014) Epigenetic silencing of miR-210 increases the proliferation of gastric epithelium during chronic Helicobacter pylori infection. *Nat. Commun.* **5**, 4497 [CrossRef Medline](#)
- Ikedo, S., Kitadate, A., Abe, F., Saitoh, H., Michishita, Y., Hatano, Y., Kawabata, Y., Kitabayashi, A., Teshima, K., Kume, M., Takahashi, N., and Tagawa, H. (2017) Hypoxia-inducible microRNA-210 regulates the DIMT1-IRF4 oncogenic axis in multiple myeloma. *Cancer Sci.* **108**, 641–652 [CrossRef Medline](#)
- Ikedo, S., Kitadate, A., Abe, F., Takahashi, N., and Tagawa, H. (2018) Hypoxia-inducible KDM3A addiction in multiple myeloma. *Blood Adv.* **2**, 323–334 [CrossRef Medline](#)
- Janker, L., Mayer, R. L., Bileck, A., Kreutz, D., Mader, J. C., Utpatel, K., Heudobler, D., Agis, H., Gerner, C., and Slany, A. (2019) Metabolic, anti-apoptotic and immune evasion strategies of primary human myeloma cells indicate adaptations to hypoxia. *Mol. Cell. Proteomics* **18**, 936–953 [CrossRef Medline](#)
- van Bui, C. P. J. J., Visser, W., and van Knippenberg, P. H. (1984) Increased translational fidelity caused by the antibiotic Kasugamycin and ribosomal ambiguity in mutants harboring the Ksga gene. *FEBS Lett.* **177**, 119–124 [CrossRef](#)
- Lafontaine, D. L., Preiss, T., and Tollervey, D. (1998) Yeast 18S rRNA dimethylase Dim1p: a quality control mechanism in ribosome synthesis? *Mol. Cell. Biol.* **18**, 2360–2370 [CrossRef Medline](#)
- White, J., Li, Z., Sardana, R., Bujnicki, J. M., Marcotte, E. M., and Johnson, A. W. (2008) Bud23 methylates G1575 of 18S rRNA and is required for efficient nuclear export of Pre-40S subunits. *Mol. Cell. Biol.* **28**, 3151–3161 [CrossRef Medline](#)
- Meyer, B., Wurm, J. P., Kotter, P., Leisegang, M. S., Schilling, V., Buchhaupt, M., Held, M., Bahr, U., Karas, M., Heckel, A., Bohnsack, M. T., Wöhnert, J., and Entian, K. D. (2011) The Bowen-Conradi syndrome protein Nep1 (Emg1) has a dual role in eukaryotic ribosome biogenesis, as an essential assembly factor and in the methylation of Psi1191 in yeast 18S rRNA. *Nucleic Acids Res.* **39**, 1526–1537 [CrossRef Medline](#)
- Létoquart, J., Huvelle, E., Wacheul, L., Bourgeois, G., Zorbas, C., Graille, M., Heurgue-Hamard, V., and Lafontaine, D. L. J. (2014) Structural and functional studies of Bud23-Trm112 reveal 18S rRNA N⁷-G1575 methylation occurs on late 40S precursor ribosomes. *Proc. Natl. Acad. Sci. USA* **111**, E5518–E5526 [CrossRef Medline](#)

30. Jack, K., Bellodi, C., Landry, D. M., Niederer, R. O., Meskauskas, A., Musalgaonkar, S., Kopmar, N., Krasnykh, O., Dean, A. M., Thompson, S. R., Ruggero, D., and Dinman, J. D. (2011) rRNA pseudouridylation defects affect ribosomalligand binding and translational fidelity from yeast to human cells. *Mol. Cell* **44**, 660–666 [CrossRef Medline](#)
31. Penzo, M., and Montanaro, L. (2018) Turning uridines around: role of rRNA pseudouridylation in ribosome biogenesis and ribosomal function. *Biomolecules* **8**, 38 [CrossRef](#)
32. Nachmani, D., Bothmer, A. H., Grisendi, S., Mele, A., Bothmer, D., Lee, J. D., Monteleone, E., Cheng, K., Zhang, Y., Bester, A. C., Guzzetti, A., Mitchell, C. A., Mendez, L. M., Pozdnyakova, O., Sportoletti, P., *et al.* (2019) Germline NPM1 mutations lead to altered rRNA 2'-O-methylation and cause dyskeratosis congenita. *Nat. Genet.* **51**, 1518–1529 [CrossRef Medline](#)
33. Larkin, M. A., Blackshields, G., Brown, N. P., Chenna, R., McGettigan, P. A., McWilliam, H., Valentin, F., Wallace, I. M., Wilm, A., Lopez, R., Thompson, J. D., Gibson, T. J., and Higgins, D. G. (2007) Clustal W and Clustal X version 2.0. *Bioinformatics* **23**, 2947–2948 [CrossRef Medline](#)
34. Hirsch, C. A., and Hiatt, H. H. (1966) Turnover of liver ribosomes in fed and in fasted rats. *J. Biol. Chem.* **241**, 5936–5940 [Medline](#)
35. Rakotondrafara, A. M., and Hentze, M. W. (2011) An efficient factor-depleted mammalian in vitro translation system. *Nat. Protoc.* **6**, 563–571 [CrossRef Medline](#)
36. Lafontaine, D., Vandenhaute, J., and Tollervey, D. (1995) The 18S rRNA dimethylase Dim1p is required for pre-ribosomal RNA processing in yeast. *Genes Dev.* **9**, 2470–2481 [CrossRef Medline](#)
37. Parsons, D. W., Jones, S., Zhang, X., Lin, J. C., Leary, R. J., Angenendt, P., Mankoo, P., Carter, H., Siu, I. M., Gallia, G. L., Olivi, A., McLendon, R., Rasheed, B. A., Keir, S., Nikolskaya, T., *et al.* (2008) An integrated genomic analysis of human glioblastoma multiforme. *Science* **321**, 1807–1812 [CrossRef Medline](#)
38. Dinman, J. D. (2006) Programmed ribosomal frameshifting goes beyond viruses: organisms from all three kingdoms use frameshifting to regulate gene expression, perhaps signaling a paradigm shift. *Microbe* **1**, 521–527 [CrossRef Medline](#)
39. Ghalei, H., Trepreau, J., Collins, J. C., Bhaskaran, H., Strunk, B. S., and Karbstein, K. (2017) The ATPase Fap7 tests the ability to carry out translocation-like conformational changes and releases Dim1 during 40S ribosome maturation. *Mol. Cell.* **67**, 990–1000 [CrossRef Medline](#)
40. Fraser, C. S., and Doudna, J. A. (2007) Structural and mechanistic insights into hepatitis C viral translation initiation. *Nat. Rev. Microbiol.* **5**, 29–38 [CrossRef Medline](#)
41. Kim, P., Zhao, J., Lu, P., and Zhao, Z. (2017) mutLBSgeneDB: mutated ligand binding site gene DataBase. *Nucleic Acids Res.* **45**, D256–D263 [CrossRef Medline](#)
42. Chen, C. W., Lin, M. H., Liao, C. C., Chang, H. P., and Chu, Y. W. (2020) iStable 2.0: predicting protein thermal stability changes by integrating various characteristic modules. *Comput. Struct. Biotechnol. J.* **18**, 622–630 [CrossRef Medline](#)
43. Defoiche, J., Zhang, Y., Lagneaux, L., Pettengell, R., Hegedus, A., Willems, L., and Macallan, D. C. (2009) Measurement of ribosomal RNA turnover in vivo by use of deuterium-labeled glucose. *Clin. Chem.* **55**, 1824–1833 [CrossRef Medline](#)
44. Vagin, A., and Teplyakov, A. (2010) Molecular replacement with MOLREP. *Acta Crystallogr. D Biol. Crystallogr.* **66**, 22–25 [CrossRef Medline](#)
45. Winn, M. D., Ballard, C. C., Cowtan, K. D., Dodson, E. J., Emsley, P., Evans, P. R., Keegan, R. M., Krissinel, E. B., Leslie, A. G., McCoy, A., McNicholas, S. J., Murshudov, G. N., Pannu, N. S., Potterton, E. A., Powell, H. R., *et al.* (2011) Overview of the CCP4 suite and current developments. *Acta Crystallogr. D Biol. Crystallogr.* **67**, 235–242 [CrossRef Medline](#)
46. Murshudov, G. N., Skubak, P., Lebedev, A. A., Pannu, N. S., Steiner, R. A., Nicholls, R. A., Winn, M. D., Long, F., and Vagin, A. A. (2011) REFMAC5 for the refinement of macromolecular crystal structures. *Acta Crystallogr. D Biol. Crystallogr.* **67**, 355–367 [CrossRef Medline](#)
47. Emsley, P., and Cowtan, K. (2004) Coot: model-building tools for molecular graphics. *Acta Crystallogr. D Biol. Crystallogr.* **60**, 2126–2132 [CrossRef Medline](#)
48. Adams, P. D., Afonine, P. V., Bunkoczi, G., Chen, V. B., Davis, I. W., Echols, N., Headd, J. J., Hung, L. W., Kapral, G. J., Grosse-Kunstleve, R. W., McCoy, A. J., Moriarty, N. W., Oeffner, R., Read, R. J., Richardson, D. C., *et al.* (2010) PHENIX: a comprehensive Python-based system for macromolecular structure solution. *Acta Crystallogr. D Biol. Crystallogr.* **66**, 213–221 [CrossRef Medline](#)
49. Laskowski, R. A., MacArthur, M. W., Moss, D. S., and Thornton, J. M. (1993) Procheck—a program to check the stereochemical quality of protein structures. *J. Appl. Crystallogr.* **26**, 283–291 [CrossRef](#)
50. Ontiveros, R. J., S. H., Stoute, J., Yanas, A., Cui, Y., Zhang, Y., and Liu, K. F. (2020) Coordination of mRNA and tRNA methylations by TRMT10A. *Proc. Natl. Acad. Sci. U S A* **117**, 7782–7791 [CrossRef](#)
51. Ran, F. A., Hsu, P. D., Wright, J., Agarwala, V., Scott, D. A., and Zhang, F. (2013) Genome engineering using the CRISPR-Cas9 system. *Nat. Protoc.* **8**, 2281–2308 [CrossRef Medline](#)
52. Sondalle, S. B., Longerich, S., Ogawa, L. M., Sung, P., and Baserga, S. J. (2019) Fanconi anemia protein FANCI functions in ribosome biogenesis. *Proc. Natl. Acad. Sci. U S A* **116**, 2561–2570 [CrossRef Medline](#)
53. Kim, D., Langmead, B., and Salzberg, S. L. (2015) HISAT: a fast spliced aligner with low memory requirements. *Nat. Methods* **12**, 357–360 [CrossRef Medline](#)
54. Lawrence, M., Huber, W., Pages, H., Aboyoun, P., Carlson, M., Gentleman, R., Morgan, M. T., and Carey, V. J. (2013) Software for computing and annotating genomic ranges. *PLoS Comput. Biol.* **9**, e1003118 [CrossRef Medline](#)
55. Love, M. I., Huber, W., and Anders, S. (2014) Moderated estimation of fold change and dispersion for RNA-seq data with DESeq2. *Genome Biol.* **15**, 550 [CrossRef Medline](#)
56. Huang da, W., Sherman, B. T., and Lempicki, R. A. (2009) Bioinformatics enrichment tools: paths toward the comprehensive functional analysis of large gene lists. *Nucleic Acids Res.* **37**, 1–13 [CrossRef Medline](#)
57. Huang, D. W., Sherman, B. T., and Lempicki, R. A. (2009) Systematic and integrative analysis of large gene lists using DAVID bioinformatics resources. *Nat. Protoc.* **4**, 44–57 [CrossRef Medline](#)